Multiple excitations in the K fluorescence emission of Mn, Fe and Ni compounds

P. Glatzel*, U. Bergmann†, F. M. F. de Groot** and S. P. Cramer†*

*University of California at Davis, USA
†Lawrence Berkeley National Laboratory, USA
**Universiteit Utrecht, The Netherlands

Abstract. The creation and the decay of a *1s* vacancy can result in the excitation of a second electron. In this paper, two different modes of *1s* core hole creation as a diagnostic tool to study multi-electron excitations in the K fluorescence emission are compared. The *1s* core hole excited state can be created either by photoionization or by radioactive K capture decay. In the latter case, a *1s* electron reacts with a proton in the nucleus to yield a neutron and an escaping electron neutrino. We report a comparison of Kβ spectra obtained from x-ray excitation in Mn and K capture in 55-Fe in various chemical environments. The K$\beta_{1,3}$ main lines of the photoexcited spectra are broader than the corresponding lines obtained after K capture and the weak satellite lines at higher energies (K$\beta_{2,5}$) differ in shape. A theoretical model on the basis of different electron relaxation depending on the mode of core-hole creation is presented.

INTRODUCTION

Any electronic transition in an atom causes a readjustment of the passive electrons, *i.e.* the electrons that are not directly involved in the transition, to the perturbed potential. A passive electron in an orbital ϕ^i_μ before the perturbation will relax into an orbital $\phi^f_{\mu'}$. For an adiabatic relaxation we have μ=μ', *i.e.* the final state orbital is described by the same set of quantum numbers. If the relaxation is non-adiabatic, the electron will occupy an orbital with different quantum numbers ($\mu \neq \mu'$). Those transitions can be referred to as shake or multiple electronic transitions.

In a two step picture that can be used to describe fluorescence emission, the excitation of a second electron can either occur during the creation or during the decay of a *1s* vacancy. Multi-electron transitions upon inner-shell vacancy creation in *3d* transition metals have been studied using photoelectron [1] and absorption spectroscopy [2, 3, 4]. In order to obtain an estimate for the fluorescence energies due to transitions from doubly ionized excited states we can use a simple Z+1 model as shown in Figure 1. For Mn we expect the KLβ lines at about 70 eV above the Kβ main lines. As an example, the KLβ lines in MnO_2 are shown. The KLβ peak intensity exhibits a slow rise over several keV as predicted by the Thomas model [5]. The spectra shown in Figure 1 are not corrected for self-absorption and we therefore do not attempt for a detailed analysis. A comprehensive treatment of the KLα lines in Cu can be found in reference [6, 7].

When the core hole is filled the excitation of a second electron can occur via a radiative Auger emission (RAE) where a photon is emitted and an electron is simultanuously

CP652, *X-Ray and Inner-Shell Processes: 19th International Conference on X-Ray and Inner-Shell Processes*
edited by A. Bianconi, A. Marcelli, and N. L. Saini

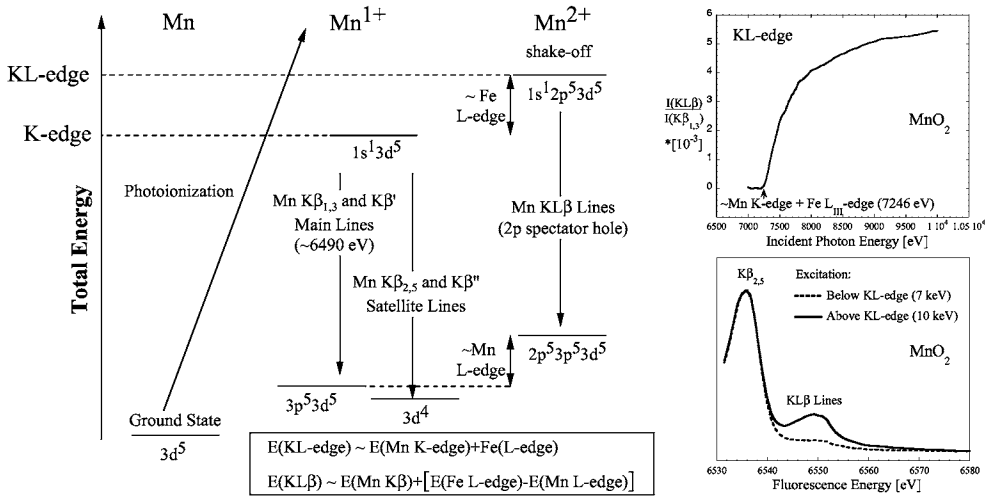

FIGURE 1. *Left: Term scheme for Kβ and KLβ emission in Mn. Atomic configurations are used and only the partly occupied orbitals are given. An estimate for the KL-edge and the KL fluorescence energy is given based on a simple Z+1 model. Right: Kβ main and satellite lines. For the latter, the fluorescence emissions following photoexcitation below (solid line) and above (dashed line) the KL-edge are shown.*

elevated into a higher orbital or into the continuum [8]. Figure 2 shows the KLL RAE in metallic Ni and in K_2NiF_6. The shake probability is related to the overlap integral between the emitting and the receiving orbital and is largest for monopole shake transitions [9]. The KLL-edge therefore resembles the K-edge and not the L-edge because it probes the p-density of unoccupied states. The Ni KLL onset is at about 880 eV below the Ni Kα lines.

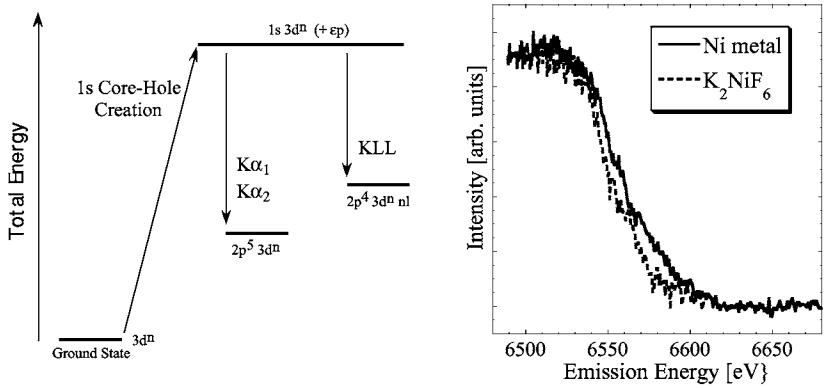

FIGURE 2. *Left: Term scheme of KLL radiative Auger emission in a 3d metal. Right: KLL edge in Ni metal and K_2NiF_6. The KLL edges differ between the metallic Ni and Ni(IV) in an ionic compound, i.e. they show a chemical dependence.*

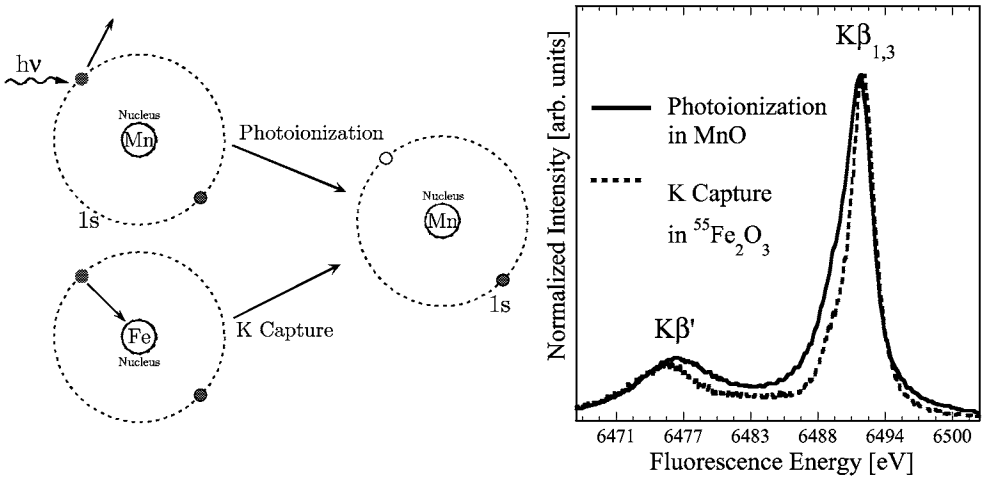

FIGURE 3. *Left: K capture in ^{55}Fe and 1s photoionization in Mn. Both processes result in an ion that has a Mn (Z=25) nucleus and a hole in the 1s shell. Right: Experimental Kβ spectra for MnO and $^{55}Fe_2O_3$. The instrumental broadening is ≈0.8 eV for both spectra. The spectra are normalized to each other in the $K\beta_{1,3}$ peak. The energy scale is the measured fluorescence energy and the spectra were not shifted in energy relative to each other.*

COMPARING DIFFERENT MODES OF 1S CORE HOLE CREATION

Kβ Main Lines

As we have seen in the previous examples, doubly excited intermediate or final states yield sufficiently shifted (*i.e.* can be separated experimentally) K fluorescence lines if the second vacancy occurs in the L or K shell. In contrast, valence electron shake transitions will result in overlapping spectral features between singly and doubly fluorescence final states. In order to tackle this problem one can compare K fluorescence spectra following two different modes of *1s* core hole creation [10, 11]. Provided that the two modes have different valence electron shake probabilities one expects different K fluorescene lines if shake transitions have considerable probability.

On the left side of Figure 3 it is shown that photoionization in Mn and radioactive electron capture decay from the K shell (K capture) lead to the formally identical fluorescence initial state with a Mn-55 nucleus and a hole in the *1s* shell. We compare on the right side of Figure 3 the Kβ main lines, that arise from *3p* to *1s* transitions, for MnO and $^{55}Fe_2O_3$. Both compounds have a metal $3d^5$ configuration in the ionic approximation. The striking difference between the two spectra is that the $K\beta_{1,3}$ peak appears sharper on the low energy side in the $^{55}Fe_2O_3$ than in the MnO spectrum than. A multiplet approach using atomic self-consistent field calculations can account for the $K\beta_{1,3}$ and $K\beta'$ features[12]. For a more detailed treatment the local symmetry (O_h for both comounds) and orbital hybridization can be taken into account [13, 14]. It is found

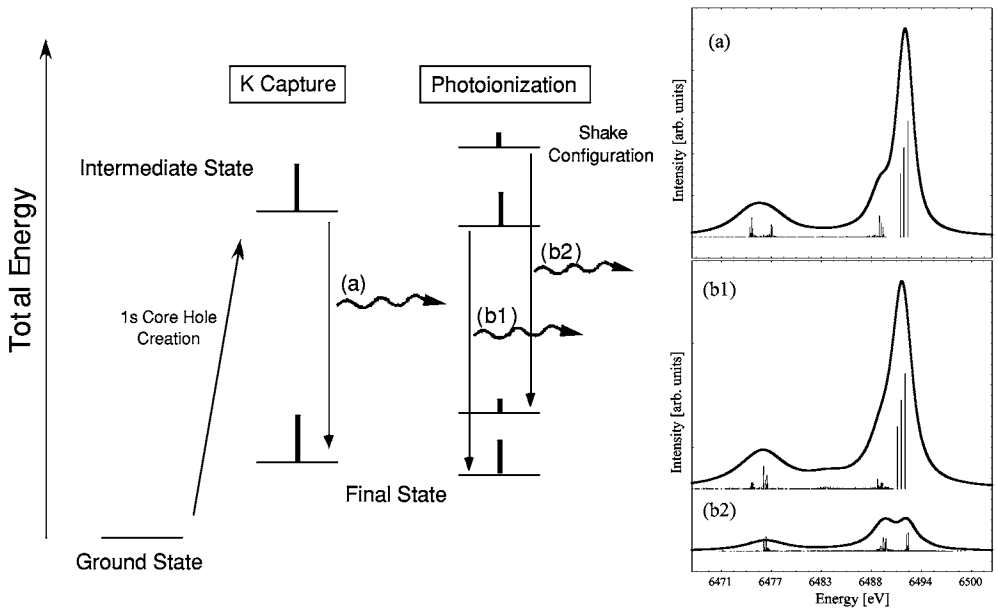

FIGURE 4. *Left: Term scheme for Kβ emission after core hole creation via K capture and photoionization, respectively. The change of effective potential upon photoionization leads to a populated shake configuration in the intermediate state. Assuming that the shake configuration does not relax into the lowest intermediate state we obtain two Kβ emitting transitions. Right: Calculated Kβ main lines after (a) K capture and (b) photoionization. For the latter the two spectra as described in the term scheme on the left are shown and the spectra are scaled according to the calculated intensities of the 1s intermediate states.*

that different hybridization and crystal field splittings between MnO and Fe_2O_3 cannot explain the differences observed in the experimental spectra [15].

Figure 4 shows how the dependence of the spectral features on the mode of *1s* core hole creation can be incorporated into a theoretical model. The change of effective potential experienced by the valence electrons after *1s* photoionization causes shake transitions and, in a simplified model, two populated intermediate states. Both states act as fluorescence initial states and give rise to Kβ emission. We therefore assume that the shake configuration in the *1s* intermediate state does not decay into the lowest *1s* intermediate state before the decay of the *1s* core hole, *i.e.* the fluorescence intial state is not fully relaxed. On the other hand, the effective potential experienced by the valence electrons hardly changes in K capture decay because a negative charge (the *1s* electron) annihilates with a positive charge (a proton in the nucleus) [15].

The calculated spectra on the right side of Figure 4 are based on atomic multiplet calculations including crystal field splitting and ligand-to-metal charge transfer [13, 15]. Two Kβ spectra are shown for MnO after photoionization. They are scaled according to the calculated population of the *1s* excited states that are reached in a photoionization process. Only one calculated Kβ spectrum is shown in the case of K capture because only one *1s* excited state is reached. Adding up the two photoionization Kβ spectra

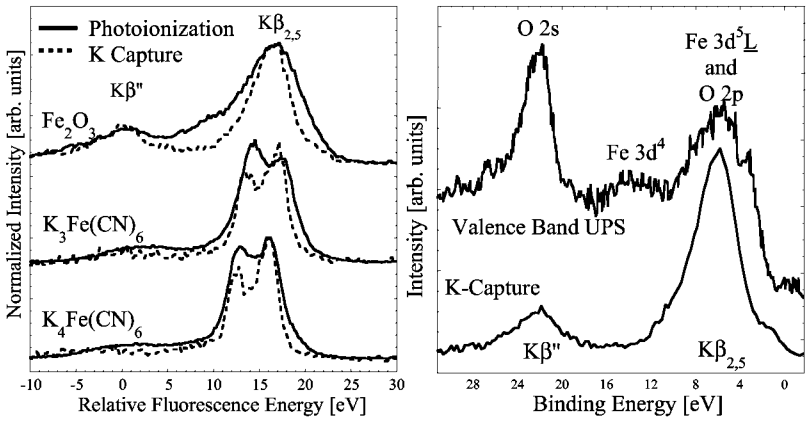

FIGURE 5. *Kβ satellite emission in Fe compounds after K capture (KC) and photoioniziation (PI). To facilitate direct comparison a common energy scale (relative fluorescence energy) is given in the bottom. The feature in Fe_2O_3 at about 0 eV relative fluorescence intensity is the Kβ″ or cross over peak. It was used to align the photoionization and K capture spectra relative to each other.*

will yield a spectrum that is broadened on the low energy side of the $K\beta_{1,3}$ peak in comparison to the K capture spectrum and thus reproduce the experimental observation [15].

Kβ Satellite Lines

Transitions from shells higher than *3p* (Kβ satellite lines) can be interpreted using density functional theory [16, 17]. The Kβ satellite lines in Fe_2O_3, $K_4Fe(CN)_6$ and $K_3Fe(CN)_6$ are shown in Figure 5. While the Kβ main lines are dominated by splittings due to intraatomic Coulomb and spin-orbit interactions whose magnitudes depend on the nuclear charge, the Kβ satellite lines are mainly shaped by ligand field effects and band formation. We therefore compared a Mn to an Fe-55 compound in the previous section and now compare identical Fe and Fe-55 compounds for the Kβ satellites. The fluorescence energy scale had to be shifted for a comparison. We used the Kβ″ peak that has been assigned to a ligand *2s* to metal *1s* transition [18] to align the K capture and photoionization spectra.

All spectral features recorded after photoionization are broader than in the data taken after K capture. Furthermore, the intensity ratios of the two bands in the $K\beta_{2,5}$ structure of the cyanides change between the two modes of excitation. The broadening indicates that more final states are populated after photoionization as we already concluded for the Kβ main lines.

On the right of Figure 5 we compare Fe_2O_3 valence band photoemission spectra (taken from reference [19]) to the $^{55}Fe_2O_3$ Kβ satellite spectra. Fujimori *et al.* interpreted the valence band UPS spectra using a ligand-to-metal charge transfer model and

assigned the strong peak at low binding energies to a screened $3d^5\underline{L}$ configuration and an O *2p* band and the weaker structure at about 14 eV binding energy to an unscreened $3d^4$ configuration. The Kβ satellite lines are dominated by transitions from orbitals with mainly O *2s* and *2p* character. These orbitals exhibit some p-character relative to the metal center and therefore serve for dipole allowed transitions to the metal *1s* shell.

ACKNOWLEDGMENTS

We thank Sandra Fiskum at PNNL for preparing the ^{55}Fe compounds. SSRL is funded by the Department of Energy, Office of Basic Energy Sciences. We are indebted to Bernd Sonntag and Jorgen Hansen for fruitful discussions. Use of the Advanced Photon Source was supported by the U.S. Department of Energy, Basic Energy Sciences, Office of Science, under contract No. W-31-109-ENG-38. BioCAT is a National Institutes of Health-supported Research Center RR-08630 This work was supported by the National Institutes of Health GM-44380 and the Department of Energy, Office of Biological and Environmental Research.

REFERENCES

1. Hüfner, S., *Photoelectron spectroscopy : principles and applications*, Springer series in solid-state sciences ; 82., Springer, 1996, 2nd edn.
2. Bianconi, A., Garcia, J., Benfatto, M., Marcelli, A., Natoli, C. R., and Ruiz-Lopez, M. F., *Phys. Rev. B, Condens. Matter (USA)*, **43**, 6885–92 (1991).
3. Bianconi, A., Chenxi, L., Campanella, F., Della Longa, S., Pettiti, I., Pompa, M., Turtu, S., and Udron, D., *Phys. Rev. B, Condens. Matter (USA)*, **44**, 4560–9 (1991).
4. Guo, J., Ellis, D. E., Goodman, G. L., Alp, E. E., Soderholm, L., and Shenoy, G. K., *Phys. Rev. B, Condens. Matter (USA)*, **41**, 82–95 (1990).
5. Thomas, T. D., *Phys. Rev. Lett. (USA)*, **52**, 417–20 (1984).
6. Deutsch, M., Gang, O., Hamalainen, K., and Kao, C. C., *Phys. Rev. Lett. (USA)*, **76**, 2424–7 (1996).
7. Fritsch, M., Kao, C. C., Hamalainen, K., Gang, O., Forster, E., and Deutsch, M., *Phys. Rev. A, At. Mol. Opt. Phys. (USA)*, **57**, 1686–97 (1998).
8. Aberg, T., *Phys. Rev. A, Gen. Phys. (USA)*, **4**, 1735–40 (1971).
9. Fujikawa, T., and Kawai, J., *J. Phys. Soc. Jpn. (Japan)*, **68**, 4032–6 (1999).
10. Mukoyama, T., and Uda, M., *Phys. Rev. A*, **61**, 030501/1–4 (2000).
11. Hansen, P. G., Jonson, B., Borchert, G. L., and Schult, O. W., *Atomic inner-shell physics*, Plenum Press, 1985, pp. 237–267.
12. Meisel, A., Leonhardt, G., and Szargan, R., *X-Ray Spectra and Chemical Binding*, vol. 37 of *Chemical Physics*, Springer-Verlag, 1989.
13. de Groot, F. M. F., Fontaine, A., Kao, C. C., and Krisch, M., *J. Phys.*, **6**, 6875–84 (1994).
14. Kotani, A., *J. Electron Spectrosc. Relat. Phenom. (Netherlands)*, **100**, 75–104 (1999).
15. Glatzel, P., Bergmann, U., de Groot, F. M. F., and Cramer, S. P., *Phys. Rev, B, Condens, Matter Mater. Phys. (USA)*, **64**, 045109/1–10 (2001).
16. Bergmann, U., Bendix, J., Glatzel, P., Gray, H. B., and Cramer, S. P., *J Chem Phys*, **116**, 2011–2015 (2002).
17. Drager, G., and Brummer, O., *Phys. Status Solidi B (East Germany)*, **124**, 11–28 (1984).
18. Bergmann, U., Horne, C. R., Collins, T. J., Workman, J. M., and Cramer, S. P., *Chem. Phys. Lett.*, **302**, 119–124 (1999).
19. Fujimori, A., Saeki, M., Kimizuka, N., Taniguchi, M., and Suga, S., *Phys. Rev. B, Condens. Matter*, **34**, 7318–28 (1986).